RADIATIVE TRANSFER MODELS FOR DERIVING GEOSTATIONARY BROADBAND SHORTWAVE RADIANCES DIRECTLY FROM VISIBLE CHANNELS FOR THE CERES SYN1DEG PRODUCT

David Doelling[a], Forrest Wrenn[b], Lusheng Liang[b]

[a]NASA Langley Research Center, Hampton, VA 23666
[b]Science Systems and Applications, Inc., Hampton, VA 23666

ABSTRACT

The Clouds and the Earth's Radiant Energy System (CERES) project was designed to observe the Earth's radiation budget at the 1° regional and global scale. The CERES instruments on the Terra (10:30 AM local equator crossing time) and Aqua (1:30 PM) satellite may not accurately capture the 24-hour mean flux over regions with systematic diurnal cycles. The Terra-only and Aqua-only derived regional monthly mean SW flux can differ by 25 Wm^{-2} over maritime stratus and land afternoon convective regions. The CERES project utilizes hourly Geostationary imager (GEO) derived broadband fluxes to more accurately estimate the regional diurnal flux in between CERES measurements. We propose an approach that converts the GEO visible radiance to broadband radiance using RTM radiances that are specific to the individual GEO visible channel spectral response functions. The RTM is first validated using the very spectrally narrow MODIS visible channel and CERES broadband radiances.

Index Terms— CERES, Geostationary derived broadband fluxes

1. INTRODUCTION

The Clouds and the Earth's Radiant Energy System (CERES) project was designed to observe the Earth's radiation budget at the 1° regional and global scale [1]. CERES releases a suite of time and spatially averaged products including: SSF1deg, SYN1deg, and EBAF. The SSF1deg product provides TOA fluxes based on single satellite measurements at their respective local equatorial crossing times from Terra or Aqua. The SYN1deg includes Terra, Aqua and hourly geostationary (GEO) measurements to better capture variations in the diurnal cycle not observed by Aqua or Terra [2]. The EBAF climate quality product takes the stability of the SSF1deg product and combines it with the diurnally complete SYN1deg product and constrains the net TOA flux to be consistent with the ocean heat storage [3].

The CERES Edition 4 derives GEO broadband fluxes from narrowband radiances by first inter-calibrating all of the GEO imager radiances with Aqua-Moderate Resolution Imaging Spectroradiometer (MODIS) to maintain a consistent calibration reference through the record [4]. The GEO visible narrowband radiances are converted to MODIS-like visible radiances using crude radiative transfer models (RTM) and then empirical models convert these MODIS-like radiances to broadband radiances [3]. The GEO broadband radiances are then converted to SW fluxes using the same angular directional models [5] that convert the CERES observed radiances into fluxes. Finally, the fluxes are then radiometrically scaled regionally to the CERES observed fluxes [3].

We present a new approach by directly converting the GEO radiances to broadband radiances based on state of the art RTMs. Skipping the intermediate step means we do not lose valuable spectral information by converting to a MODIS-like visible radiance, since most GEOs over the CERES record have visible channels that are spectrally broader than MODIS. The new RTMs are a function of atmospheric profile, cloud phase, optical thickness, and cloud height. The first step is to convolve the RTM hyperspectral radiances with the GEO visible channel spectral response and the complete broadband spectra. The RTM based GEO narrowband and broadband radiances are saved as look up tables (LUT) and are used to convert the observed GEO narrowband radiances to broadband radiances. In order to validate the RTM radiances, they are compared to the coincident observed Aqua MODIS and CERES footprint radiances.

2. METHODOLOGY

2.1. The shortwave radiative transfer model (RTM)

A DIScrete Ordinate Radiative Transfer (DISORT) model is used to generate ~ 2500 shortwave (0.2µm to 5µm) spectral radiances. It is similar to the RTM that CERES uses to unfilter the broadband radiances. The absorption of seven major gases (H_2O, O_3, O_2, CH_4, CO_2, CO and NO) are based on the HITRAN 2008 database of the LBLRTM code. The ocean surface relies on Cox-Munk using 4 wind speeds. The land surface BRDF model is based on the Ross-Li BRDF model using 10-years of MODIS observations provided by the MCD43C1 product according to IGBP type. For water clouds, a log-normal particle size distribution is used to define the single scattering albedo, asymmetry factor and phase function for a given effective particle size and optical depth. A two habit ice model is used to define the ice cloud properties defined by the effective diameter and optical

depth (Ping Yang personal communication). Maritime, continental and dust aerosol models at 8 optical depths are employed. McClatchy standard tropical, midlatitude summer and winter atmospheric profiles are incorporated. The water cloud is located between 2 to 4-km, whereas the ice cloud extent is between 9-11 km.

2.1. Spectral convolution and band reflectance LUT

The CERES project has used 18 GEO imagers beginning in the year 2000. The RTM hyper-spectral radiances are convolved with each of the 18 GEO, MODIS 0.65µm and 0.86µm, and VIRS 0.65µm spectral response function (SRF). The GEO visible band RTM LUT reflectances are then stratified by solar zenith, view zenith, relative azimuthal angle, cloud phase, optical depth, and particle size as well as clear-sky, atmosphere profile and surface type. A perfect broadband spectral response is assumed to build the broadband RTM LUT reflectances.

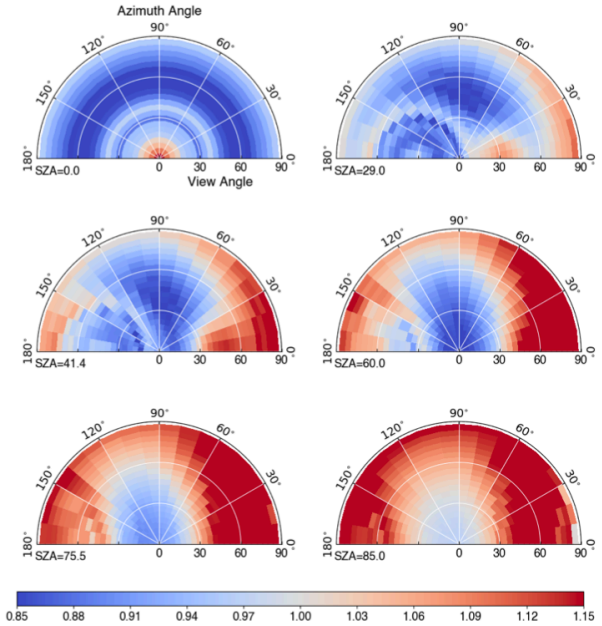

Fig. 1. MODIS 0.65µm visible divided by the broadband reflectance view zenith and azimuth polar plots as a function of solar zenith angle (SZA) for tropical ocean water cloud with an optical depth 1, a particle size of 20 µm, and an ocean speed of 5 m/s. View zenith angle (VZA) (distance) and relative azimuth angle (RAZ) (angle) define the coordinates of the polar plot. Forward scatter = 0°. Glint is located at the center of the SZA=0 plot and at VZA=30°, RAZ=0°, and SZA=29°.

The ratio of the visible band and broadband reflectance is then the adjustment factor required to convert the observed GEO, MODIS, or VIRS visible band reflectance to a broadband reflectance. The MODIS visible to broadband angular reflectance ratios are shown in Fig. 1. The ratio is highly dependent on the solar, view and azimuthal angles. As the path length increases the broadband absorption increases, therefore increasing the ratio. Glint also has a relatively large ratio and is located in the forward direction where the view and solar angles are similar. However, for optically thick ice clouds the ratio is very similar across all angles, since they are spectrally flat, Lambertian, and located at the top of the atmosphere (not shown).

The first generation GEO's encompass both the visible and NIR spectra, where much of the NIR water vapor absorption bands reside (see Fig. 2 Meteosat-7). The 2nd generation GEOs (GOES 8-15) SRF only observe the visible wavelengths. Greater spectral coverage of older GEO imager visible channels captures a greater portion of broadband spectra than the visible imagers aboard newer GEOs. We hypothesize that the broader SRFs decrease the uncertainty when deriving the broadband flux. The latest 3rd generation GEOs (GOES 16-17) contain multiple solar reflected bands (RSB), where the individual bands are very narrow. While it is advantageous to use multiple SW channels, we first validate the limits of the RTM by using a single visible channel. This accomplished by using the simultaneous MODIS 0.65µm band and CERES broadband measurements from the Aqua satellite.

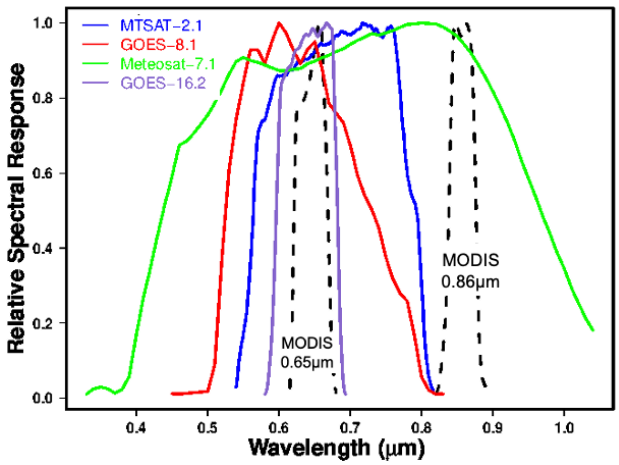

Fig. 2. GEO (solid lines) and MODIS (dashed lines) spectral response functions. Meteosat-7 (green) is a first generation GEO, GOES-8 (red) and MTSAT-2 (blue) are second generation GEOs, whereas GOES-16 channel 2 (purple) is a third generation GEO. Note how the spectral bands are becoming increasingly narrow over time and more similar to MODIS.

3. VALIDATION

The RTM LUT is validated by using MODIS and CERES radiances, which are coincident, collocated, co-angled, from the Aqua-CERES Ed4 SSF footprint level 2 product. The CERES footprint has a nominal size of 20-km and is sub-divided by clear and two cloud layers. Each of the sub-footprint MODIS reflectances are converted to the

broadband reflectance separately using the RTM LUTs. The sub-footprint broadband reflectances are then area weighted and compared to the CERES footprint radiance. Rather than using the MODIS cloud optical depth, the MODIS reflectance is converted to broadband reflectance, based on the linear regression of the RTM MODIS reflectances with the RTM CERES reflectances. Fig. 3 illustrates the linearity of the RTM based MODIS and CERES reflectances. This avoids possible artifacts due to inconsistent optical depth retrievals across the many GEOs in the CERES record.

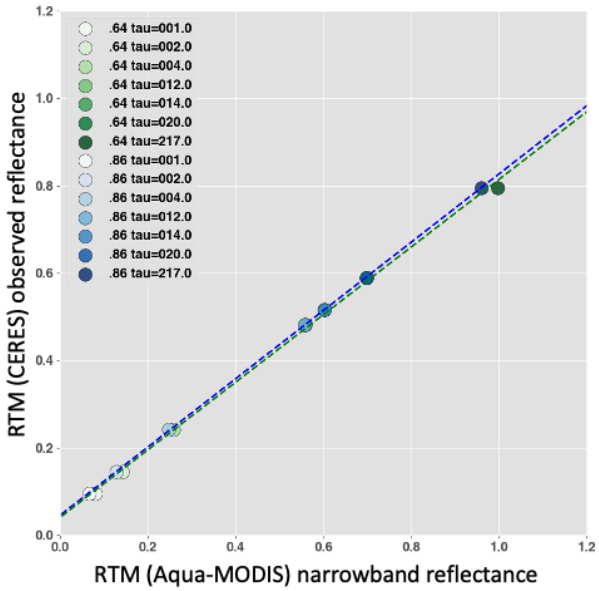

Fig. 3. The RTM Aqua-MODIS 0.64μm (green dots) and 0.86 μm (blue dots) and RTM CERES broadband reflectance as a function optical depth for an ice cloud located between 9-17-km within a tropical profile with an ice particle diameter of 115μm for SZA=29°, VZA=16° and RAZ=130°. Note the linearity of the reflectances with respect to optical depth.

The RTM predicted from Aqua-MODIS 0.64μm channel and CERES observed broadband radiances were compared over ocean regions during January 2010 and is shown in Fig. 2. The average regional (1° by 1° latitude by longitude) bias and RMS error was 1.701% and 6.932%, respectively. The clear-sky regions in the Arabian Sea seem to have a positive bias and a large RMS error. Mid-latitude storm tracks, maritime stratus west of Chile, and tropical western Pacific deep convective clouds have lower RMS errors than their surroundings. This is probably due to the fact that the brighter the cloud the more Lambertian it is. High solar zenith angles observed near 50° latitude have a negative bias. The MODIS 0.86μm channel have a bias and RMS errors of 4.0% and 9.0%, respectively, slightly higher than the 0.64μm band. The 0.86μm band is located in the NIR, where strong water vapor absorption bands are found. These results were based on the McClatchy tropical atmosphere with clouds having an ice and water particle diameter of 115μm and 50μm, which may exceed the observed particle sizes. Next we recompute the LUT tables with various ice and water particle sizes.

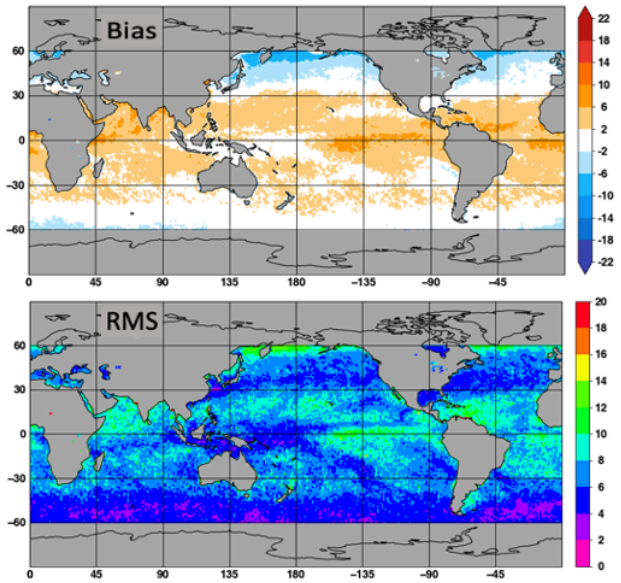

Fig. 4. The bias (%) and RMS error (%) of the Aqua-MODIS 0.64μm derived from RTM and CERES observed broadband radiances during January 2010.

Table 1. The bias (%) and RMS error (%) of the Aqua-MODIS 0.64μm derived from RTM and CERES observed broadband radiances during January 2010 as a function of water and ice particle diameter for footprints with water or ice cloud amounts greater than 90%. The bias and RMS error are also listed for clear-sky conditions (cloud amount less than 10%) and all-sky (see Fig. 4).

MODIS	0.65μm		0.86 μm	
	Bias %	RMS %	Bias %	RMS %
Water Cloud				
8 μm	6.5	8.8	7.4	9.6
20 μm	4.8	7.4	7.2	9.8
32 μm	3.0	6.6	6.5	9.4
50 μm	1.9	6.1	5.8	8.8
Ice Cloud				
21.86 μm	10.1	11.7	9.4	12.9
46.34 μm	8.1	9.6	8.0	11.6
115.32 μm	4.2	6.2	5.9	9.8
Clear-sky	0.2	6.4	3.2	11.6
All-sky	1.7	7.0	4.0	9.0

In order to determine the optimal RTM particle size that best converts the MODIS channel narrowband radiances into broadband radiances, LUTs are produced for a water cloud particle radii of 8μm, 16μm, 32μm, and 50μm. Only footprints with a water cloud amount greater than 90% are used to validate the RTM. Results are found in

Table 1. Both the bias and RMS error are reduced as the effective particle size is increased for both the 0.64µm and 0.86µmm channels. Similarly, the ice cloud particle diameter was varied and validated for footprints with ice cloud fraction greater than 90%. Ice clouds have a more dramatic reduction in bias and RMS error with particle size, especially for the 0.64µm channel.

To validate the RTM hyper-spectral radiance by wavelength, they are compared to observed SCanning Imaging Absorption SpectroMeter for Atmospheric CHartographY (SCIAMACHY) hyper-spectral reflectances onboard the sun-synchronous ENVISAT satellite (10 ECT) [6]. The SCIAMACHY conditions are matched as much as possible to the RTM conditions using the NASA-Langley SCIAMACHY Spectra Plot tool [7]. Fig. 5 shows that the SCIAMACHY refletances most closely follow the RTM 32 µm water particle diameter reflectances. For ice clouds, the SCIAMACHY reflectances follows the 115µm mostly, except for wavelengths greater than 1.4 µm, where it straddles the 115µm and 46µm RTM reflectances. The RTM LUTs will be optimized by adjusting the cloud layer, PW, atmospheric column, particle sizes to best predict the CERES TOA reflectances

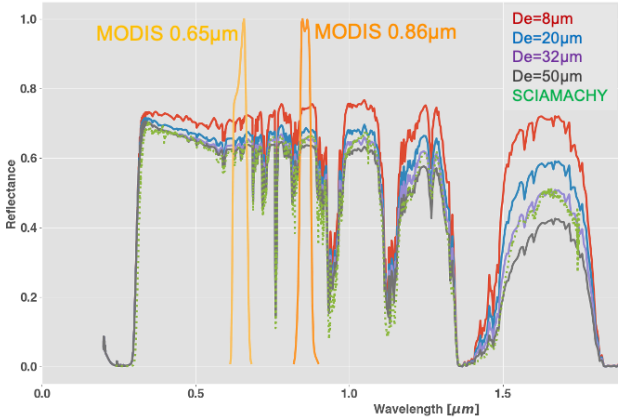

Fig. 5. The RTM water cloud reflectance as a function of particle diameter for SZA=29°, VZA=16° and RAZ=130° with an optical depth of 20. The MODIS 0.65µm and 0.86µm spectral response functions are plotted in orange. SCIAMACHY hyper-spectral reflectances are plotted as green dots. Note how the SCIAMACHY hyper-spectral reflectances follow the 32µm RTM reflectances.

4. CONCLUSIONS

A new GEO visible channel to broadband radiance conversion approach has been presented, which preserves the spectral information contained within the individual GEO SRFs, by utilizing state of the art hyper-spectral RTM radiances. The RTM visible to broadband radiance conversion LUTs are validated against coincident MODIS visible and CERES broadband measured radiances. The RTM radiances will also be validated against the Visible Infrared Radiometer (VIRS) and CERES radiances onboard the Tropical Rainfall Measuring Mission (TRMM) satellite, which is in a precessionary orbit. Once the RTM LUTs sufficiently predict the TOA reflectances, the GEO specific LUTs will be validated using coincident GEO and CERES measurements as well as Meteosat Spinning Enhanced Visible and Infrared Imager (SEVIRI) visible and Geostationary Earth Radiation Budget (GERB) broadband fluxes

5. ACKNOWLEDGEMENT

The authors also thank the CERES, GERB, and Megha-Tropiques, science teams for their insightful temporal averaging discussions. These data were obtained from the NASA Langley Research Center EOSDIS Distributed Active Archive Center.

6. REFERENCES

[1] Wielicki, B. A., B. R. Barkstrom, E. F. Harrison, R. B. Lee III, G. L. Smith, and J. E. Cooper, 1996: Clouds and the Earth's Radiant Energy System (CERES): An Earth Observing System experiment. Bull. Amer. Meteor. Soc., 77, 853–868.

[2] Doelling, D., N. Loeb, D. Keyes, M. Nordeen, D. Morstad, C. Nguyen, B. Wielicki, D. Young, and M. Sun, 2013: Geostationary Enhanced Temporal Interpolation for CERES flux products. *J. Atmos. Oceanic Technol*. Vol. 30, No. 6, June 2013: 1072-1090, doi:10.1175/JTECH-D-12- 00136.1

[3] Loeb, Norman G.; Doelling, David R.; Wang, Hailan; Su, Wenying; Nguyen, Cathy; Corbett, Joseph G.; Liang, Lusheng; Mitrescu, Cristian; Rose, Fred G.; Kato, Seiji (2018) Clouds and the Earth's Radiant Energy System (CERES) Energy Balanced and Filled (EBAF) Top-of-Atmosphere (TOA) Edition 4.0 Data Product, *Journal of Climate*, 31, 895-918, https://doi.org/10.1175/JCLI-D-17-0208.1

[4] Doelling, D.R., C. Haney, R. Bhatt, B. Scarino, A. Gopalan, Geostationary Visible Imager Calibration for the CERES SYN1deg Edition 4 Product, *Remote Sens.* **2018**, *10*(2), 288; https://doi.org/10.3390/rs10020288

[5] Loeb, N., N. Manalo-Smith, S. Kato, W. F. Miller, S. K. Gupta, P. Minnis, and B. A. Wielicki, 2003: Angular distribution models for top-of-atmosphere radiative flux estimation from the Clouds and the Earth's Radiant Energy System instrument on the Tropical Rainfall Measuring Mission Satellite. Part I: Methodology. J. Appl. Meteor., 42, 240–265.

[6] H. Bovensmann, J. P. Burrows, M. Buchwitz, J. Frerick, S. Noël, V. V. Rozanov, K. V. Chance, and A. P. H. Goede, "SCIAMACHY: Mission objectives and measurement modes," J. Atmos. Sci., vol. 56, no. 2, pp. 127-150, Jan. 1999

[7] B. R. Scarino, D. R. Doelling, P. Minnis, A. Gopalan, T. Chee, R. Bhatt, C. Lukashin, and C. O. Haney, "A web-based tool for calculating spectral band difference adjustment factors derived from SCIAMACHY hyperspectral data," IEEE Trans. Geosci. Remote Sens., vol. 54, no. 5, pp. 2529-2542, 2016.